

FUSE OBSERVATIONS OF INTRINSIC ABSORPTION IN THE SEYFERT 1 GALAXY MRK 509

G. A. KRISS^{1,3}, R. F. GREEN², M. BROTHERTON², W. OEGERLE³, K. R. SEMBACH³, A. F. DAVIDSEN³, S. D. FRIEDMAN³, M. E. KAISER³, W. ZHENG³, B. WOODGATE⁴, J. HUTCHINGS⁵, J. M. SHULL⁶ D. G. YORK⁷

To appear in ApJ Letters

ABSTRACT

We present far-ultraviolet spectra of the Seyfert 1 galaxy Mrk 509 obtained in 1999 November with the Far Ultraviolet Spectroscopic Explorer (FUSE). Our data span the observed wavelength range 915–1185 Å at a resolution of ~ 20 km s⁻¹. The spectrum shows a blue continuum, broad O VI $\lambda\lambda 1032, 1038$ emission, and a broad C III $\lambda 977$ emission line. Superposed on these emission components, we resolve associated absorption lines of O VI $\lambda\lambda 1032, 1038$, C III $\lambda 977$, and Lyman lines through L ζ . Seven distinct kinematic components are present, spanning a velocity range of -440 to $+170$ km s⁻¹ relative to the systemic velocity. The absorption is clustered in two groups, one centered at -370 km s⁻¹ and another at the systemic velocity. The blue-shifted cluster may be associated with the extended line emission visible in deep images of Mrk 509 obtained by Phillips et al. Although several components appear to be saturated, they are not black at their centers. Partial covering or scattering permits $\sim 7\%$ of the broad-line or continuum flux to be unaffected by absorption. Of the multiple components, only one has the same ionization state and column density as highly ionized gas that produces the O VII and O VIII ionization edges in X-ray spectra of Mrk 509.

Subject headings: Galaxies: Active — Galaxies: Individual (Mrk 509) — Galaxies: Nuclei — Galaxies: Quasars: Absorption Lines — Galaxies: Seyfert — Ultraviolet: Galaxies — X-Rays: Galaxies

1. INTRODUCTION

Mrk 509 straddles the boundary in luminosity between Seyfert 1 nuclei and QSOs with an absolute magnitude of $M_B = -22.0$. This gives it particular importance for understanding how the properties typical of the well-studied nearby active galactic nuclei (AGN) might scale with luminosity, and, therefore, be applied to the more distant and luminous QSOs. Like many Seyfert 1 galaxies, Mrk 509 exhibits intrinsic UV absorption lines (York et al. 1984; Crenshaw, Boggess, & Wu 1995; Savage, Sembach, & Lu 1997; Crenshaw et al. 1999) and X-ray absorption edges of O VII and O VIII (Reynolds 1997; George et al. 1998). The UV absorption is blue-shifted relative to the systemic velocity of 10,365 km s⁻¹ (Phillips et al. 1983), and Phillips et al. suggest that it is related to the expanding shell of high ionization gas visible in images and spectra out to a radius of 15'' from the nucleus.

At high resolution, UV absorption in Seyferts appears to be kinematically complex (NGC 3516: Crenshaw, Maran, & Mushotzky 1998; NGC 5548: Mathur, Elvis, & Wilkes 1999), with at most one of the UV components having any possible relation to the X-ray absorbing gas (Mathur, Elvis, & Wilkes 1999). High resolution observations of UV absorption lines covering a range of ionization states is the key to determining which, if any, of the UV absorbers are associated with an X-ray warm absorber. The FUSE observations of Mrk 509 we present in this paper extend the far-UV spectral coverage to wavelengths shortward of 1200 Å. Our spectra include the O VI $\lambda\lambda 1032, 1038$ resonance doublet and the high-order Ly-

man lines, down to the redshifted Lyman limit. Since the Ly α lines resolved in earlier UV observations are saturated, the high-order lines visible with FUSE provide a better constraint on the total neutral hydrogen column density. The O VI doublet is a crucial link for establishing a connection between the higher ionization absorption edges seen in the X-ray and the lower ionization absorption lines seen in earlier UV observations. Based on these new observations, we discuss the implications for the location of the absorbing gas in AGN, and how intrinsic absorption in low- z AGN may be related to the broad-absorption line phenomenon in more luminous QSOs.

2. OBSERVATIONS

FUSE comprises four separate primary mirrors gathering light for four prime-focus, Rowland-circle spectrographs and two, two-dimensional, photon-counting detectors. For a full description of FUSE, its mission, and its in-flight performance, see Moos et al. (2000), and Sahnow et al. (2000). Two of the optical systems employ LiF coatings on the optics, giving coverage from ~ 990 –1187 Å, and the other two use SiC coatings, which provide reflectivity down to wavelengths as short as 905 Å. The mirror systems focus light on a slit assembly in the focal plane. The holographically ruled gratings disperse the light entering through the slits and form an astigmatic image on the two-dimensional microchannel-plate detectors. The detectors have KBr photocathodes and delay-line anode readouts that provide the location and arrival time of each photon event.

Mrk 509 was observed on 1999 Nov 9 and 1999 Nov 11 through the 30'' \times 30'' low-resolution apertures. We obtained

¹Space Telescope Science Institute, 3700 San Martin Drive, Baltimore, MD 21218; gak@stsci.edu

²Kitt Peak National Observatory, National Optical Astronomy Observatories, P.O. Box 26732, 950 North Cherry Ave., Tucson, AZ, 85726-6732

³Center for Astrophysical Sciences, Department of Physics and Astronomy, The Johns Hopkins University, Baltimore, MD 21218–2686

⁴Laboratory for Astronomy and Solar Physics, Code 681, NASA/Goddard Space Flight Center, Greenbelt, MD 20771

⁵Dominion Astrophysical Observatory, National Research Council of Canada, Victoria, BC, V8X 4M6, Canada; john.hutchings@hia.nrc.ca

⁶CASA and JILA, Department of Astrophysical and Planetary Sciences, University of Colorado, Campus Box 389, Boulder, CO 80309; mshull@casa.colorado.edu

⁷Department of Astronomy, University of Chicago, Chicago, IL 60637; don@oddjob.uchicago.edu

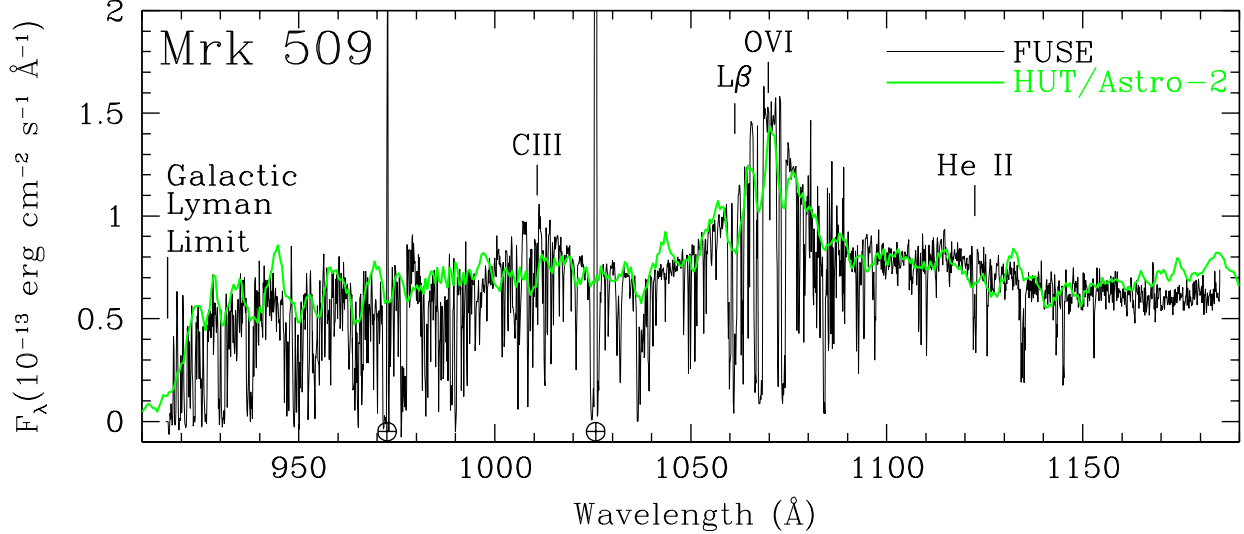


FIG. 1.— FUSE spectrum of Mrk 509 (binned by 20 pixels) is shown as a thin black line. Hopkins Ultraviolet Telescope (HUT) data obtained during the Astro-2 mission in 1995 March (scaled by a factor of 0.69) are shown as the green curve.

good spectra from the LiF1 and LiF2 channels covering the 987–1187 Å band, and lower signal-to-noise-ratio (S/N) spectra from the SiC2 channel covering 905–1091 Å. As a result of channel misalignment during the observations, almost no data were obtained in the SiC1 channel. We recorded the data in photon-address mode, which provides a time-tagged list of event positions in the down-linked data stream. This enables us to filter out short periods of event “bursts” (Sahnow et al. 2000) and to correct for image motion on the detectors to achieve the best spectral resolution. As described by Sahnow et al. (2000), we extracted one-dimensional spectra from the two-dimensional data on each of the active detector segments. These extracted spectra are dark subtracted and flux and wavelength calibrated by the standard FUSE calibration pipeline. We estimate that the flux scale is accurate to $\sim 10\%$, and that wavelengths are accurate to $\sim 15 \text{ km s}^{-1}$. Poisson errors and data quality flags are propagated through the data reduction process along with the science data.

To produce the full spectrum shown in Figure 1, we have spliced together sections of data from segments SiC2A, LiF1A, SiC2B, LiF1B, and LiF2A to eliminate the gaps in wavelength coverage and to present the best S/N. These data have also been binned by 20 pixels (0.12 Å) to show the overall appearance of the spectrum. In our analysis discussed in the following sections, we use spectra binned by only 5 pixels. This preserves the full spectral resolution of $\sim 20 \text{ km s}^{-1}$ for this observation.

In Figure 1 strong, broad O VI emission is readily apparent as is broad C III $\lambda 977$ emission. Another less prominent feature in the spectrum is the hump of emission redward of O VI $\lambda\lambda 1032, 1038$. We have marked the position of He II $\lambda 1085$, but one can see that its wavelength is a bit too long. A similar feature was noted in the spectra of low-redshift quasars by Laor et al. (1995) who suggested this may be blended Fe II emission. The numerous Galactic absorption features, particularly H₂, make the intrinsic spectrum difficult to see shortward of 1000 Å, but, at the resolution of FUSE, one can trace out the intrinsic spectrum as the peaks between the foreground absorptions. Note how the C III $\lambda 977$ line is not prominent in the overlayed Hopkins Ultraviolet Telescope (HUT) data, primarily because the foreground Galactic absorption renders it less visible at the $\sim 3\text{\AA}$ resolution of HUT.

3. WARM ABSORBING GAS IN MRK 509

A detailed examination of the FUSE spectrum at full spectral resolution shows that absorption near the redshift of Mrk 509 is visible in the Lyman lines, in the O VI $\lambda\lambda 1032, 1038$ resonance doublet, and in C III $\lambda 977$. Figure 2 shows portions of the Mrk 509 spectrum around each absorption line complex with velocities relative to the AGN systemic velocity.

Close inspection of the O VI doublet and the Lyman lines shows that while much of the absorption appears to be saturated, the absorption troughs are not black. (Scattered light in FUSE at these levels is negligible. See Sahnow et al. 2000.) Partial covering by the absorbers or scattering around the absorbing region can explain this appearance. Extended broad-line Balmer emission and variable, polarized broad Balmer-line emission are seen in Mrk 509 (Mediavilla et al. 1998; Thompson & Martin 1988; Young et al. 1999). These are both indications that scattering may play some role in producing the light at the bottoms of the absorption troughs.

In the L β and O VI absorption lines we have identified at least 7 distinct kinematic components spanning a range of velocities from -478 to $+166 \text{ km s}^{-1}$ relative to the systemic velocity of Mrk 509. To ascertain the physical properties of these intrinsic absorbers in Mrk 509, we fit a model to the spectral regions surrounding the O VI lines, the Lyman lines, and C III $\lambda 977$ using the IRAF task `specfit` (Kriss 1994). Figure 3 shows the best fit overlayed on the L β /O VI region. Our model of the emission components includes an underlying power-law continuum, a pair of broad (FWHM $\sim 11,000 \text{ km s}^{-1}$) O VI emission lines with their relative intensities fixed at the optically thin ratio of 2:1, a pair of narrow (FWHM $\sim 1200 \text{ km s}^{-1}$) O VI emission lines, again with their relative intensities fixed at a 2:1 ratio, and a broad L β emission line with its width and velocity linked to those of the broad O VI lines. The absorption lines are treated as Gaussians in optical depth, and they are allowed to partially cover the emission components with fraction f_c . The wavelengths of the O VI doublets are linked at the ratio of their laboratory values, their velocity widths are required to be identical, and their relative optical depths are fixed at a 2:1 ratio. Thus, a pair of lines uniquely determines the column density and the covering fraction for a given kinematic component. The L β lines have their wavelengths linked to those of the O VI lines, but, to allow for residual uncertainties in the FUSE wavelength

scale, we permit a linear adjustment to the whole group of $L\beta$ lines. The widths and the covering fractions for the $L\beta$ lines are fixed at the values determined for the O VI lines.

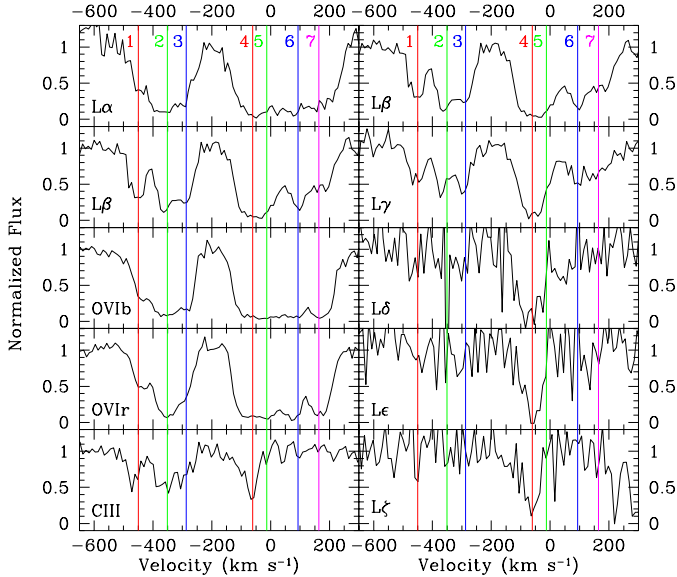


FIG. 2.— Normalized line profiles for the Lyman lines, C III λ 977, O VI λ 1032 (OVIb), and O VI λ 1038 (OVIr) are shown. These data are binned by 5 pixels, and foreground Galactic absorption features have been divided out. The central wavelengths of the 7 distinct intrinsic absorption components are marked. The L α profile at the upper left is archival HST data from a GHRS observation by B. Savage.

Higher-order Lyman lines are visible in the FUSE spectrum out to L ζ . These lines are also fit simultaneously with L β . Their optical depths are fixed at the ratio of their oscillator strengths to that of L β , their wavelengths are linked to those of O VI at the ratio of the vacuum wavelengths (again allowing for slight linear adjustments), and their widths are fixed at the same values as those of the O VI components. The Lyman lines permit an independent check of the covering fractions determined from the O VI doublets. We find that if they are allowed to vary independently, they give results consistent with those determined from O VI alone, so we leave them fixed at the O VI values in our final results. C III λ 977 is treated similarly. Although there is no independent check on its covering fraction, we also fixed f_c at the O VI values.

The results of our fits for C III λ 977, L β , and O VI λ 1032 are given in Table 1. The column densities for each ion are determined by integrating the optical depth across each parameterized line profile. (Since the parameters given completely determine the values for O VI λ 1038 and the remaining Lyman lines, these are not shown.)

To determine physical conditions in the absorption components, we used photoionization models similar to those used by Krolik & Kriss (1995) and Kriss et al. (1996). From a grid of models we determined the total column density and the ionization parameter based on the observed relative columns of H I and O VI. With no other constraints, this method can lead to double-valued results for the ionization parameter and column density since the ratio of O VI to H I will rise to a peak and then decline. However, we note that the presence of C III in components 1–4 restricts the solutions to the lower ionization parameter in these cases. Component 5 lies near the peak of the N(O VI)/N(H I) curve, and, as we show below, the inferred ionization and column density are corroborated by X-ray

observations of O VII and O VIII. As component 5 fully accounts for the observed X-ray absorption, a high-column, high-ionization-parameter solution for components 6 and 7 is also ruled out by the X-ray observations. Physical parameters for the 7 kinematic components are shown in Table 2. Note that most components have relatively low total column densities and ionization parameters. The components associated with the most blue-shifted complex could well be associated with the outflowing narrow-emission line gas as originally suggested by Phillips et al. (1983). This would place it many kiloparsecs from the central ionizing source. Similarly, the lower ionization components (6 & 7) near the systemic velocity may be associated with the low-ionization gas in the rotating disk near the center of Mrk 509 (Phillips et al. 1983).

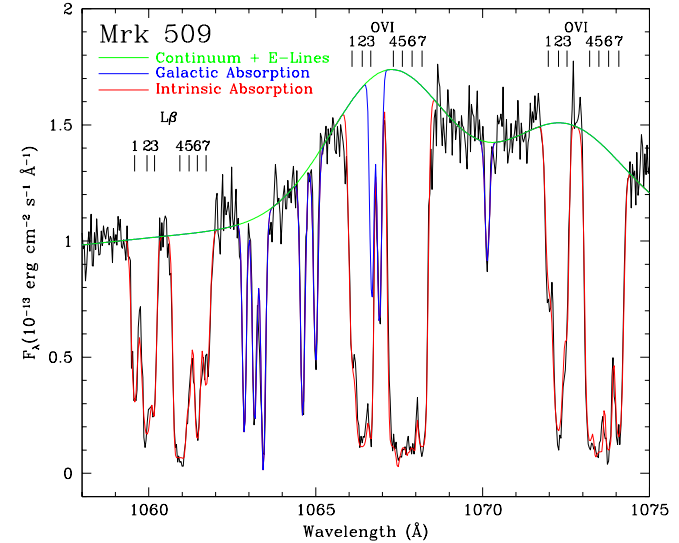


FIG. 3.— FUSE spectrum of Mrk 509 (binned by 5 pixels) in the L β /O VI region is shown as the thin black line. The best fit described in the text is overlaid in color. The thin green line shows the fitted continuum and emission components. The thin red line shows the fitted intrinsic absorption components, and the thin blue line shows the foreground Galactic absorption lines. The central wavelengths of the 7 distinct intrinsic absorption components are marked.

Among all the absorption components, the most exceptional is #5. Its high ionization parameter and high total column density make it likely to be directly associated with the intrinsic X-ray warm absorber. In his analysis of the ASCA X-ray spectrum of Mrk 509, Reynolds (1997) found O VII and O VIII optical depths of $0.11^{+0.03}_{-0.04}$ and $0.04^{+0.04}_{-0.03}$, respectively. For threshold photoionization cross sections of $\sigma_{O7} = 0.239 \times 10^{-18} \text{ cm}^2$ and $\sigma_{O8} = 0.109 \times 10^{-18} \text{ cm}^2$ (Reilman & Manson 1979), this implies column densities of $N_{O7} = (4.6^{+1.3}_{-1.7}) \times 10^{17} \text{ cm}^{-2}$ and $N_{O8} = (3.7^{+3.7}_{-2.8}) \times 10^{17} \text{ cm}^{-2}$. Our photoionization modeling for UV absorption component 5 predicts $N_{O7} = 2.3 \times 10^{17} \text{ cm}^{-2}$ and $N_{O8} = 0.1 \times 10^{17} \text{ cm}^{-2}$. Considering the large uncertainties in the X-ray columns and the temporal difference between the X-ray and UV observations, the agreement is remarkably close. The X-ray absorption predicted by our photoionization modeling for the other UV absorption components is negligible.

We conclude that observations of the O VI doublet in AGN is a perfect complement to observations of the O VII and O VIII edges often seen in the X-ray spectra of Seyfert 1 galaxies. Comparison of the UV and X-ray measurements permits us to rigorously test whether the gas responsible for X-ray absorption in Seyferts also gives rise to the UV absorption, as suggested by Mathur et al. (1994, 1995). The multiple kinematic compo-

nents, the wide range of ionization parameters, and the typical low total columns inferred for most of the UV absorbers (see Kriss et al. 1996; Crenshaw et al. 1999) make it unlikely that the UV and X-ray absorption arise in the same gas. In fact, in Mrk 509, with the high spectral resolution and far-UV sensitivity of FUSE, we can easily pick out the high ionization absorption component that is likely to be directly associated with the X-ray absorbing gas. The remaining components (which dominate the total UV absorption) are lower column density and lower ionization. This suggests that the absorbing medium is complex, with separate UV and X-ray dominant zones. One potential geometry is high density, low column UV-absorbing clouds embedded in a low density, high ionization medium that dominates the X-ray absorption. This is possibly a wind driven off the obscuring torus or the accretion disk.

TABLE 1
ABSORPTION LINES IN MRK 509

Feature	#	W_λ (Å)	N_{ion} (cm $^{-2}$)	Δv^a (km s $^{-1}$)	FWHM (km s $^{-1}$)	f_c
C III $\lambda 977.02$	1	0.11	1.6×10^{13}	-438	49	0.77
	2	0.21	2.4×10^{13}	-349	63	0.91
	3	0.06	5.4×10^{12}	-280	31	1.00
	4	0.17	2.1×10^{13}	-75	57	0.92
	5	< 0.01	< 2.0×10^{12}	-5	40	0.92
	6	< 0.01	< 2.0×10^{12}	+71	48	0.94
	7	< 0.01	< 2.0×10^{12}	+166	59	0.94
H I $\lambda 1025.72$	1	0.25	5.7×10^{14}	-438	49	0.77
	2	0.24	5.3×10^{14}	-349	63	0.91
	3	0.26	9.3×10^{14}	-280	31	1.00
	4	0.43	6.0×10^{15}	-75	57	0.92
	5	0.36	2.7×10^{14}	-5	40	0.92
	6	0.25	1.2×10^{15}	+71	48	0.94
	7	0.28	1.2×10^{15}	+166	59	0.94
O VI $\lambda 1031.93$	1	0.24	1.9×10^{14}	-438	49	0.77
	2	0.46	1.3×10^{15}	-349	63	0.91
	3	0.14	1.2×10^{14}	-280	31	1.00
	4	0.44	1.2×10^{15}	-75	57	0.92
	5	0.31	3.2×10^{15}	-5	40	0.92
	6	0.37	1.2×10^{15}	+71	48	0.94
	7	0.41	9.4×10^{14}	+166	59	0.94

^aVelocity relative to a systemic redshift of $cz = 10365$ km s $^{-1}$ (Phillips et al. 1983).

One puzzling inconsistency with the outflow hypothesis, however, is that component 5 is at rest with respect to the systemic velocity. If the X-ray absorbing gas is in the low-ionization disk observed by Phillips et al. (1983), then the low line-of-sight velocity could be explained by having most of its motion transverse to the line of sight. The ionization parame-

ter $U \sim 0.4$ is consistent with this location if the gas density is low enough—for $n = 10^3$ cm $^{-3}$ and an ionizing luminosity of $L_{\text{ion}} = 3.4 \times 10^{45}$ erg s $^{-1}$ for Mrk 509, the absorbing gas would be located at a distance of 330 pc from the nuclear source, or $\sim 0.5''$ for $H_0 = 65$ km s $^{-1}$ Mpc $^{-1}$. Setting better constraints on the location of the X-ray absorbing gas, however, will require better knowledge of the gas density, which can be determined from variability studies (e.g., Kriss et al. 1997; Hamann, Barlow, & Junkkarinen 1997; Espey et al. 1998).

TABLE 2
PHYSICAL PROPERTIES OF THE ABSORBERS IN MRK 509

#	$N_{\text{OVI}}/N_{\text{HI}}$	N_{tot} (cm $^{-2}$)	$\log U$
1	0.37	2.0×10^{18}	-1.64
2	1.51	5.9×10^{18}	-1.19
3	0.48	2.2×10^{18}	-1.79
4	0.19	1.6×10^{19}	-1.73
5	13.9	5.0×10^{20}	-0.43
6	2.14	7.6×10^{18}	-1.41
7	2.76	6.8×10^{18}	-1.46

4. SUMMARY

The far-UV spectrum of the Seyfert 1 galaxy Mrk 509 shows bright broad O VI $\lambda\lambda 1032, 1038$ emission as well as broad C III $\lambda 977$ emission. Kinematically complex intrinsic absorption in Mrk 509 shows at least 7 distinct components in the Lyman lines, O VI $\lambda\lambda 1032, 1038$, and C III $\lambda 977$. Although many of the O VI and Lyman line components appear to be saturated, they are not black, implying that partial covering or scattering affects the absorption. Only one of the intrinsic absorption components in Mrk 509 is likely to be associated with the warm X-ray absorbing gas. Component 5 (near the systemic velocity) has an ionization state and column density that is in reasonable agreement with the O VII and O VIII absorption edges seen in the ASCA X-ray spectrum. The high resolution of FUSE and its sensitivity in the O VI band make it an ideal tool for identifying high-ionization UV absorbers that may correspond to X-ray warm absorbers.

This work is based on data obtained for the Guaranteed Time Team by the NASA-CNES-CSA FUSE mission operated by the Johns Hopkins University. Financial support to U. S. participants has been provided by NASA contract NAS5-32985. G. Kriss acknowledges additional support from NASA Long Term Space Astrophysics grant NAGW-4443.

REFERENCES

Crenshaw, D.M., Boggess, A., and Wu, C.-C. 1995, AJ, 110, 1026
 Crenshaw, D. M., Kraemer, S. B., Boggess, A., Maran, S. P., Mushotzky, R. F., Wu, C.-C. 1999, ApJ, 516, 750
 Crenshaw, D.M., Maran, S.P., & Mushotzky, R.F. 1998, ApJ, 496, 797
 Espey, B.R., Kriss, G.A., Krolik, J. H., Zheng, W., Tsvetanov, Z., & Davidsen, A.F. 1998, ApJ, 500, L13
 George, I. M., Turner, T. J., Netzer, H., Nandra, K., Mushotzky, R. F., & Yaqoob, T. 1998, ApJS, 114, 73
 Hamann, F., Barlow, T. A., & Junkkarinen, V. 1997, ApJ, 478, 87
 Kriss, G. A. 1994, in *Astronomical Data Analysis Software and Systems III*, A.S.P. Conf. Series, V. 61, ed. D. R. Crabtree, R. J. Hanisch & J. Barnes (San Francisco: ASP), 437
 Kriss G. A., et al. 1996, ApJ, 467, 622
 Kriss, G., Krolik, J., Grimes, J., Tsvetanov, Z., Zheng, W., & Davidsen, A. 1997, in proc. IAU Colloquium 159, A.S.P. Conf. Series, V. 113, ed. B.M. Peterson, F.-Z. Cheng, & A.S. Wilson (San Francisco: ASP), 453
 Krolik, J. H., & Kriss, G. A. 1995, ApJ, 447, 512
 Laor, A., Bahcall, J. N., Jannuzi, B. T., Schneider, D. P., & Green, R. F. 1995, ApJS, 99, 1
 Mathur, S., Elvis, M., & Wilkes, B. 1999, ApJ, 519, 605
 Mathur, S., Wilkes, B., & Elvis, M. 1995, ApJ, 452, 230
 Mathur, S., Wilkes, B., Elvis, M., & Fiore, F. 1994, ApJ, 434, 493
 Mediavilla, E., Arribas, S., Garcia-Lorenzo, & del Burgo, C. 1998, ApJ, 494, L9
 Moos, H. W., et al. 2000, ApJ, this issue
 Phillips, M. M., Baldwin, J. A., Atwood, B., & Carswell, R. F. 1983, ApJ, 274, 558
 Reilman, R. F., & Manson, S. T. 1979, ApJS, 40, 815
 Reynolds, C. S. 1997, MNRAS, 286, 513
 Sahnho, D., et al. 2000, ApJ, this issue
 Savage, B.D., Sembach, K.R., & Lu, L. 1997, AJ, 113, 2158
 Thompson, I. B., & Martin, P. G. 1988, ApJ, 330, 121
 York, D.G., et al. 1984, ApJ, 276, 92
 Young, S., et al. 1999, MNRAS, 303, 227